INTERNATIONAL JOURNAL FOR NUMERICAL METHODS IN FLUIDS
Int. J. Numer. Meth. Fluids **26**: 791–809 (1998)

TVD SCHEMES FOR OPEN CHANNEL FLOW

A.I. DELIS* AND C.P. SKEELS

Department of Mathematics, University of the West of England, Frenchay Campus, Bristol, BS16 1QY, UK

SUMMARY

The Saint Venant equations for modelling flow in open channels are solved in this paper, using a variety of total variation diminishing (TVD) schemes. The performance of second- and third-order-accurate TVD schemes is investigated for the computation of free-surface flows, in predicting dam-breaks and extreme flow conditions created by the river bed topography. Convergence of the schemes is quantified by comparing error norms between subsequent iterations. Automatically calculated time steps and entropy corrections allow high CFL numbers and smooth transition between different conditions. In order to compare different approaches with TVD schemes, the most accurate of each type was chosen. All four schemes chosen proved acceptably accurate. However, there are important differences between the schemes in the occurrence of clipping, overshooting and oscillating behaviour and in the highest CFL numbers allowed by a scheme. These variations in behaviour stem from the different orders and inherent properties of the four schemes. © 1998 John Wiley & Sons, Ltd.

KEY WORDS: open channel; subcritical and supercritical flows; TVD schemes

1. INTRODUCTION

In this paper, numerical schemes for solving the Saint Venant equations, which model bulk channel flow, are presented. This set of hyperbolic equations yields discontinuous solutions, which can be difficult to represent accurately without the use of a modern shock-capturing method. There are problems with the high level of truncation errors when using first-order upwind schemes and with the oscillatory behaviour of most higher-order schemes. However, coupling a total variation diminishing (TVD) interpolation with an appropriate Riemann solver, yields a high-order-accurate scheme which numerically captures discontinuities with sharp corners and avoids unrealistic oscillations.

The myriad of TVD schemes may be categorised into algebraic and geometric approaches. Further subdivisions of the algebraic schemes are symmetric, upwind and predictor-corrector. One scheme has been chosen from each of these forms of TVD schemes. The schemes used were a second-order symmetric, an upwind scheme called the modified flux, the two step TVD–McCormack and the third-order MUSCL representing the geometric approach.

Comparison of numerical schemes has a long tradition; here we summarise our experience with these numerical schemes and suggestions for further work are provided.

* Correspondence to: Department of Mathematics, University of the West of England, Frenchay Campus, Bristol, BS16 1QY, UK.

CCC 0271–2091/98/070791–19$17.50
© 1998 John Wiley & Sons, Ltd.
Received July 1996
Revised January 1997

2. GOVERNING EQUATIONS

One-dimensional unsteady flow of water in a channel of slowly varying cross-section with a sufficiently gentle bottom slope, is governed by the Saint Venant equations [1], which express conservation of mass and momentum. For flows in a prismatic channel of arbitrary cross-section, they can be written as

$$\frac{\partial \mathbf{U}}{\partial t} + \frac{\partial \mathbf{F}(\mathbf{U})}{\partial x} = \mathbf{G}, \tag{1}$$

where

$$\mathbf{U} = (A, Q)^{\tau}, \tag{2}$$

$$\mathbf{F}(\mathbf{U}) = \left(Q, \frac{Q^2}{A} + gI\right)^{\tau}, \tag{3}$$

$$\mathbf{G} = (0, gA(S_0 - S_f))^{\tau}, \tag{4}$$

where A is the wetted cross-sectional area, Q is the flow rate, I is the hydrostatic pressure force, g is the acceleration due to gravity, S_0 is the bed slope, and S_f is the friction slope. The friction slope S_f is defined, in terms of Manning's roughness coefficient n, as

$$S_f = \frac{Q^2 n^2}{A^2 R^{4/3}}, \tag{5}$$

with $R = A/P$, where P is the wetted perimeter.

The hydrostatic pressure force term may be expressed as

$$I = \int_0^{h(x,t)} (h - \eta) b(x, \eta)\, \mathrm{d}\eta,$$

where h is the water depth, η is the integration variable indicating distance from the channel bottom, and $b(x, \eta)$ is the channel width at distance η from the channel bottom:

$$b(x, \eta) = \frac{\partial A(x, \eta)}{\partial \eta}. \tag{6}$$

The hydrostatic pressure force for rectangular channels is

$$I = \frac{A^2}{2B},$$

where B is the constant channel width, and the wetted perimeter for rectangular channels is $P = 2A/B + B$.

The governing equations are based on the assumptions of hydrostatic-pressure distribution, incompressibility of water and a sufficiently small channel slope. The homogeneous part of the system is hyperbolic and responsible for most of the difficulties when it is numerically integrated; namely, the non-linearity of the flux vector $\mathbf{F}$ may lead to spontaneous discontinuities (jumps) which may have real physical meaning.

The flux vector $\mathbf{F}$ is related to the flow variables $\mathbf{U}$ through the Jacobian $\mathbf{J}$ of $\mathbf{F}$ with respect to $\mathbf{U}$ as

$$\frac{\partial \mathbf{U}}{\partial t} + \mathbf{J} \frac{\partial \mathbf{U}}{\partial x} = 0, \tag{7}$$

© 1998 John Wiley & Sons, Ltd.

and

$$\mathbf{J} = \frac{\partial \mathbf{F}}{\partial \mathbf{U}} = \begin{bmatrix} 0 & 1 \\ gA/b - u^2 & 2u \end{bmatrix}. \tag{8}$$

The hyperbolic nature of the equations ensures that matrix **J** has a complete set of independent and real eigenvectors, expressed as

$$\mathbf{e}^{1,2} = (1, u \pm c)^{\tau},$$

where velocity $u = Q/A$, and celerity $c = \sqrt{gA/b}$. The eigenvalues of **J** are given by

$$a^{1,2} = u \pm c,$$

and correspond to the two characteristic speeds with their signs providing information about the direction of flow.

3. APPROXIMATE RIEMANN PROBLEM

Higher-order modern shock-capturing schemes have been extended from the non-linear scalar case to one-dimensional non-linear systems, based on the use of Riemann solvers. In this paper, the discussion and numerical comparisons concentrate on the use of high-resolution TVD schemes with the approximate Riemann solver introduced by Roe [2].

To obtain an approximate solution of Equation (1) using a finite difference method, the domain of integration is discretised as (x_i, t_n), where: $x_i = i\Delta x$, $i = 1, 2, \ldots$ and $t_n = n\Delta t$, $n = 1, 2, \ldots$; Δt is the time increment; Δx is the grid size in space and suppose that $\mathbf{U}_i^n$ is some approximation to $\mathbf{U}(x_i, t_n)$. Godunov [3] was first to develop the idea of advancing the solution to the next time level by solving a set of Riemann problems. The Riemann problem for any system of conservation laws arises if the initial data is prescribed as two constant states ($\mathbf{U} = \mathbf{U}_L$, for $x < 0$, $\mathbf{U} = \mathbf{U}_R$ for $x > 0$). Godunov supposed that the initial data could be replaced by piecewise constant set of states for each interface $\{x_{i+1/2}\}$. Thus, the Riemann problem can be solved with $\mathbf{U}_L = \mathbf{U}_i$ and $\mathbf{U}_R = \mathbf{U}_{i+1}$, where $\mathbf{U}_i$, $\mathbf{U}_{i+1}$ denote approximations to **U** at the left and right of the cell. This gives an exact solution to the approximate problem, assuming that Δt is small enough so that the waves from neighbouring interfaces do not interact.

Roe's approximation is based on the assumption that the Jacobian matrix **J** of the flux function **F** is constant for non-linear systems in each interval ($x_i = x_{i+1}$). It is then a question of constructing an appropriate Jacobian matrix in terms of $\mathbf{U}_i$ and $\mathbf{U}_{i+1}$ in each computational cell so that the shock-capturing is automatic.

3.1. Approximate Jacobian

An approximate Jacobian is defined for the conservative flux splitting, following Roe [2], where exact solutions to the following approximate problem were considered:

$$\frac{\partial \mathbf{U}}{\partial t} + \tilde{\mathbf{J}} \frac{\partial \mathbf{U}}{\partial x} = 0, \tag{9}$$

where $\tilde{\mathbf{J}}$ is the approximate Jacobian. For each computational cell, $\tilde{\mathbf{J}}$ is chosen such that it satisfies the following conditions

(a) A linear mapping from flow vector **U** to flux vector **F** is possible,

© 1998 John Wiley & Sons, Ltd.

(b) $\tilde{\mathbf{J}}_{i+1/2}\Delta_{i+1/2}\mathbf{U} = \Delta_{i+1/2}\mathbf{F}$ where $\tilde{\mathbf{J}}_{i+1/2} = \tilde{\mathbf{J}}(\mathbf{U}_i, \mathbf{U}_{i+1})$,
(c) $\tilde{\mathbf{J}}(\mathbf{U}, \mathbf{U}) = \mathbf{J}(\mathbf{U}) = \partial\mathbf{F}(\mathbf{U})/\partial\mathbf{U}$,
(d) $\tilde{\mathbf{J}}$ has real eigenvalues and a complete set of linearly independent eigenvectors, where the operator $\Delta_{i+1/2}(\bullet) = (\bullet)_{i+1} - (\bullet)_i$.

These conditions for $\tilde{\mathbf{J}}$ ensure conservative properties and consistency with the governing equations. From condition (d) it follows that we are looking for a matrix that has approximate eigenvalues and eigenvectors of the form

$$\tilde{a}^{1,2}_{i+1/2} = \tilde{u}_{i+1/2} \pm \tilde{c}_{i+1/2},$$

$$\tilde{\mathbf{e}}^{1,2}_{i+1/2} = (1, \tilde{a}^{1,2}_{i+1/2})^{\tau},$$

and the problem of finding $\tilde{\mathbf{J}}$ is now transferred to that of finding the average values of $\tilde{u}$ and $\tilde{c}$ that meet the requirements (a)–(d).

Let $\mathbf{R}_{i+1/2}$ denote the right eigenvectors matrix then, $\tilde{\mathbf{J}}$, since it has independent and real eigenvectors, can be expressed in its diagonal form

$$\tilde{\mathbf{J}} = \mathbf{R}_{i+1/2}\,\mathrm{diag}(\tilde{a}^k_{i+1/2})\mathbf{R}^{-1}_{1+1/2} \quad k = 1, 2. \tag{10}$$

Condition (d) implies that

$$\Delta_{i+1/2}\mathbf{U} = \sum_{k=1}^{2} \alpha^k_{i+1/2}\,\tilde{\mathbf{e}}^k_{i+1/2}, \tag{11}$$

which means that the jump in states across the kth wave is given by the product of the kth wave strength $\alpha^k_{i+1/2}$ and the appropriate component of the right eigenvector. Vector Equation (11) gives

$$\alpha^{1,2}_{i+1/2} = \frac{[\Delta_{i+1/2}Q + (-\tilde{u}_{i+1/2} \pm \tilde{c}_{i+1/2})\Delta_{i+1/2}A]}{\pm 2\tilde{c}_{i+1/2}}. \tag{12}$$

From condition (a) and Equation (10), the flux difference splitting can be obtained across the two waves present in the Riemann problem as

$$\Delta_{i+1/2}\mathbf{F} = \sum_{k=1}^{2} \alpha^k_{i+1/2}\tilde{a}^k_{i+1/2}\tilde{\mathbf{e}}^k_{i+1/2}. \tag{13}$$

From Equations (12) and (13), momentarily dropping the subscript indexes, the following equation for $\tilde{u}$ and $\tilde{c}$ is obtained

$$\tilde{u}^2\Delta A - 2\tilde{u}\Delta Q + \Delta(Q^2/A) = \tilde{c}^2\Delta A - g\Delta I. \tag{14}$$

By setting

$$\tilde{c}^2 = g\frac{\Delta I}{\Delta A}, \tag{15}$$

a quadratic equation for the average velocity is obtained as

$$\tilde{u}^2\Delta A - 2\tilde{u}\Delta Q + \Delta(Q^2/A) = 0, \tag{16}$$

the solution of which is

$$\tilde{u}_{i+1/2} = \frac{Q_{i+1}/\sqrt{A_{i+1}} + Q_i/\sqrt{A_i}}{\sqrt{A_{i+1}} + \sqrt{A_i}}, \tag{17}$$

© 1998 John Wiley & Sons, Ltd.

which is the *square root averaging* of Roe [1]. When the values of two adjacent cross-sections are equal, their hydrostatic pressure distribution is the same, therefore, $\tilde{c}$ is not defined by Equation (15). By performing the limiting process, the following formula for $\tilde{c}$ is found

$$\tilde{c}^2_{i+1/2} = \begin{cases} g\frac{I_{i+1}-I_i}{A_{i+1}-A_i} & \text{if} \quad A_{i+1}-A_i \neq 0 \\ c_i^2 = c_{i+1}^2 & \text{if} \quad A_{i+1}-A_i = 0, \end{cases}$$

which is consistent with property (c).

It follows from Equation (17) that an appropriate average for A would be

$$\tilde{A}_{i+1/2} = \sqrt{A_{i+1}A_i}. \tag{18}$$

Glaister [4] replaces the geometric by the arithmetic mean. The numerical experiments shown here show that both give similarly good results.

4. TOTAL VARIATION DIMINISHING SCHEMES

The concept of TVD schemes was introduced by Harten [5]. For certain types of equations these algorithms ensure that the total variation does not increase with time, that is

$$\sum_i \left|\Delta_{i+1/2}\mathbf{U}^{n+1}\right| \leq \sum_i \left|\Delta_{i+1/2}\mathbf{U}^n\right|. \tag{19}$$

Therefore, no spurious oscillations are generated. The solution can be second- or third-order-accurate in non-critical sections, but switches to first-order at extreme.

Following Yee [6], a rather large class of TVD schemes are devised, and a few special cases are highlighted for our tests. For comparison purposes, all the TVD schemes in this study are implemented with the previously described Riemann solver, following Yee's local characteristic approach. A general form of an explicit numerical scheme can be written as

$$\mathbf{U}_i^{n+1} = \mathbf{U}_i^n - \lambda[\tilde{\mathbf{F}}^n_{i+1/2} - \tilde{\mathbf{F}}^n_{i-1/2}] + (\Delta t)\tilde{\mathbf{G}}^n_i, \tag{20}$$

where $\lambda = \Delta t/\Delta x$. The numerical flux vectors, $\tilde{\mathbf{F}}^n_{i\pm1/2}$, and the source term averages, $\tilde{\mathbf{G}}^n_i$, depend on the schemes.

The numerical flux for the general scheme (20) can be written in the form

$$\tilde{\mathbf{F}}_{i\pm1/2} = \frac{1}{2}[\mathbf{F}_i + \mathbf{F}_{i\pm1} + \mathbf{R}_{i\pm1/2}\mathbf{D}_{i\pm1/2}], \tag{21}$$

where $\mathbf{R}_{i\pm1/2}$ is the right-eigenvector matrix corresponding to the approximated Jacobian $\tilde{\mathbf{J}}$, as constructed in Section 3 and $\mathbf{D}_{i\pm1/2}$ is the scheme-dependent vector function.

The contribution of the terms in non-conservative form, e.g. physical source terms, are added separately without the limiting procedures of TVD. It is important to note that the TVD properties have never been proved for a system of non-linear equations with source terms. $\tilde{\mathbf{G}}^n_i$ is approximated by the arithmetic average of $\tilde{\mathbf{G}}^n_{i\pm1/2}$ and $\tilde{\mathbf{G}}^n_{i-1/2}$, which in turn are calculated using averages of wetted areas $\tilde{A}$, velocity $\tilde{u}$ and channel breadth $\tilde{B}$, using exact values of the bed slope S_0. The TVD–McCormack has its own method of incorporating source terms.

For each computational cell using Equations (4) and (5) along with the average velocity calculated in (17) and the assumption that the channel is locally rectangular, a natural approximation of the source term, at each computational cell, is

© 1998 John Wiley & Sons, Ltd.

$$\tilde{\mathbf{G}}^n_{i\pm 1/2} = \left[0,\, g\tilde{A}_{i\pm 1/2}S_0 - g\tilde{A}_{i\pm 1/2}\tilde{u}^2_{i\pm 1/2}n^2\left(\frac{\tilde{A}_{i\pm 1/2}}{2\tilde{A}_{i\pm 1/2}/\tilde{B}_{i\pm 1/2} + \tilde{B}_{i\pm 1/2}}\right)^{-4/3}\right]^{\tau}, \tag{22}$$

where the geometric mean for $\tilde{A}$ as in Equation (18) has been used, and following Glaister [4] $\tilde{B}^n_{i+1/2} = 1/2(B_{i+1} + B_i)$.

4.1. Second-order symmetric TVD scheme (symmetric)

The elements of the vector $\mathbf{D}_{i+1/2}$, denoted by $(d^k_{i+1/2})^s$ for the second-order symmetric TVD scheme are:

$$(d^k_{i+1/2})^s = -\lambda(\tilde{a}^k_{i+1/2})^2 L^k_{i+1/2} - \psi(\tilde{a}^k_{i+1/2})[\alpha^k_{i+1/2} - L^k_{i+1/2}], \quad k = 1, 2. \tag{23}$$

The function ψ is the entropy correction to the eigenvalues $|a^k_{i+1/2}|$ and is of the form:

$$\psi(a) = \begin{cases} |a| & |a| \geq \delta \\ (a^2 + \delta^2)/2\delta & |a| < \delta, \end{cases} \tag{24}$$

where δ is a small positive number whose value must be determined for each individual problem. Harten and Hyman [7] suggest the following formula for δ that eliminates trial procedure:

$$\delta_{i+1/2} = \max[0,\, \tilde{a}_{i+1/2} - a_i,\, a_{i+1} - \tilde{a}_{i+1/2}], \tag{25}$$

$$\delta_{i-1/2} = \max[0,\, \tilde{a}_{i-1/2} - a_{i-1},\, a_i - \tilde{a}_{i-1/2}]. \tag{26}$$

This entropy function is employed in each scheme to ensure compatibility while guaranteeing satisfaction of the energy inequality.

The limiter functions $L^k_{i\pm 1/2}$ control the second-order terms so that a smooth non-oscillatory result is guaranteed, even in the presence of discontinuities. The limiter function $L^k_{i\pm 1/2}$ is expressed in terms of wave-strengths as

$$L^k_{i+1/2} = \text{minmod}(\alpha^k_{i-1/2},\, \alpha^k_{i+1/2}) + \text{minmod}(\alpha^k_{i+1/2},\, \alpha^k_{i+3/2}) - \alpha^k_{i+1/2}, \tag{27}$$

where

$$\text{minmod}(x, y) = \text{sgn}(x)\max\{0, \min[|x|,\, y\ \text{sgn}(x)]\}.$$

Other limiters can be found in the literature [6]. For consistency, a variation of this minmod limiter is used throughout this paper; slight variations of the limiter are required for each scheme.

4.2. Second-order upwind TVD schemes (modified flux)

The second-order (space and time) TVD scheme, sometimes referred to as the modified-flux approach, was originally developed by Harten [8]. The Yee [6] modification is less diffusive and easier to implement than Harten's. Yee's modified version will be described here.

The elements of $\mathbf{D}_{i+1/2}$ in Equation (21), denoted by $(d^k_{i+1/2})^u$, are

$$(d^k_{i+1/2})^u = \sigma(\tilde{a}^k_{i+1/2})(L^k_{i+1} + L^k_i) - \psi(\tilde{a}^k_{i+1/2} + \gamma^k_{i+1/2})\alpha^k_{i+1/2}, \quad k = 1, 2. \tag{28}$$

The function $\sigma(\alpha) = 1/2(\psi(\alpha) - \lambda\alpha^2)$ and

$$\gamma^k_{i+1/2} = \begin{cases} \sigma(\tilde{a}^k_{i+1/2})(L^k_{i+1} - L^k_i)/\alpha^k_{i+1/2} & \alpha^k_{i+1/2} \neq 0 \\ 0 & \alpha^k_{i+1/2} = 0 \end{cases}.$$

The limiter function L^k_i can be expressed as

© 1998 John Wiley & Sons, Ltd.

$$L_i^k = \text{minmod}(\alpha_{i+1/2}^k, \alpha_{i-1/2}^k).$$

4.3. Predictor-corrector TVD scheme (TVD–McCormack)

The presented scheme is based on McCormack's two-step procedure. A third step equips the scheme with TVD properties, while retaining second-order-accuracy in space and time for continuous regions [6,9]. Following Garcia-Navarro [10] the scheme can be written as:

$$\mathbf{U}_i^{(1)} = \mathbf{U}_i^n - \lambda(\mathbf{F}_{i+1}^n - \mathbf{F}_i^n) + (\Delta t)\mathbf{G}_i^n, \tag{29}$$

$$\mathbf{U}_i^{(2)} = \mathbf{U}_i^n - \lambda(\mathbf{F}_{i+1}^{(1)} - \mathbf{F}_i^{(1)}) + (\Delta t)\mathbf{G}_i^{(1)}. \tag{30}$$

The solution for the next time level is

$$\mathbf{U}_i^{n+1} = \frac{1}{2}(\mathbf{U}_i^{(1)} + \mathbf{U}_i^{(2)}) + \frac{1}{2}[\bar{R}_{i+1/2}\bar{\mathbf{D}}_{i+1/2} - \bar{R}_{i-1/2}\bar{\mathbf{D}}_{i-1/2}], \tag{31}$$

where the elements of $\bar{\mathbf{D}}_{i+1/2}$ are

$$(d_{i+1/2}^k)^{PC} = \psi(\tilde{a}_{i+1/2}^k)[1 - \lambda|\tilde{a}_{i+1/2}^k|][1 - L_{i+1/2}^k]\alpha_{i+1/2}^k, \quad k = 1, 2. \tag{32}$$

Several forms of the limiting function can be found in the literature [11]. Here the minmod limiter was used, but within this context:

$$L_{i+1/2}^k = \max(0, \min(1, r_{i+1/2}^k)),$$

where

$$r_{i+1/2}^k = \frac{\alpha_{i+1/2-s}^k}{\alpha_{i+1/2}^k} \quad \text{and} \quad s = \text{sgn}(a_{i+1/2}^k),$$

$\bar{R}_{i+1/2}$ and $\bar{\mathbf{D}}_{i+1/2}$ can be evaluated at $\mathbf{U}^n$ or $\mathbf{U}^{(2)}$. In this study the $\mathbf{U}^n$ values were used.

4.4. The MUSCL scheme

The MUSCL–TVD interpolation formula, extended by Van Leer [12] provides a one-parameter family of second-order schemes and one third-order scheme. TVD properties are guaranteed for the geometric approach using a slope rather than flux limiter, which limits the gradients of the dependent variables. The MUSCL scheme involves replacing the arguments, $\mathbf{U}_{i+1}$ and $\mathbf{U}_i$, of the numerical fluxes by $\mathbf{U}_{i+1/2}^{\mathbf{R}}$ and $\mathbf{U}_{i+1/2}^{\mathbf{L}}$, where $\mathbf{U}^{\mathbf{R}}$ and $\mathbf{U}^{\mathbf{L}}$ are calculated as follows:

$$\mathbf{U}_{i+1/2}^{\mathbf{L}} = \mathbf{U}_i + \frac{1}{4}[(1-m)\Delta_{i-1/2}^+ + (1+m)\Delta_{i+1/2}^-], \tag{33}$$

$$\mathbf{U}_{i+1/2}^{\mathbf{R}} = \mathbf{U}_{i+1} - \frac{1}{4}[(1-m)\Delta_{i+3/2}^- + (1+m)\Delta_{i+1/2}^+], \tag{34}$$

where

$$\Delta_{i+1/2}^- = \text{minmod}(\Delta_{i+1/2}\mathbf{U}, \beta\Delta_{i-1/2}\mathbf{U}),$$

$$\Delta_{i+1/2}^+ = \text{minmod}(\Delta_{i+1/2}\mathbf{U}, \beta\Delta_{i+3/2}\mathbf{U}),$$

and β is a compression parameter whose value is generally in the range

$$1 \le \beta \le \frac{3-m}{1-m}, \quad \text{with } m \ne 1.$$

© 1998 John Wiley & Sons, Ltd.

The spatial order of accuracy is determined by the value of m, in this study $m = 1/3$, giving third-order-accuracy, is used.

The second-order numerical flux, analogous to Equation (21) can be expressed as

$$\tilde{\mathbf{F}}_{i+1/2} = \frac{1}{2}[\mathbf{F}(\mathbf{U}^{\mathbf{R}}_{i+1/2}) + \mathbf{F}(\mathbf{U}^{\mathbf{L}}_{i+1/2}) + \hat{R}_{i+1/2}\hat{\mathbf{D}}_{i+1/2}], \tag{35}$$

where the elements of $\hat{\mathbf{D}}_{i+1/2}$ are

$$\hat{d}^k_{i+1/2} = -\psi(\hat{a}^k_{i+1/2})\hat{\alpha}^k_{i+1/2}, \quad k = 1, 2.$$

Here $\hat{a}^k_{i+1/2}$, $\hat{R}_{i+1/2}$ and $\hat{\alpha}^k_{i+1/2}$ are evaluated as before (Section 3), but the arguments $\mathbf{U}_{i+1}$ and $\mathbf{U}_i$ have been replaced by $\mathbf{U}^{\mathbf{R}}_{i+1/2}$ and $\mathbf{U}^{\mathbf{L}}_{i+1/2}$, respectively.

5. NUMERICAL RESULTS AND DISCUSSION

The four schemes described in the previous sections were applied to two different types of channel flow. The frictionless case is represented by the idealised dam-break flood wave propagation in a channel, used in various papers when comparing schemes for modelling open channel flow. However, the most demanding tests for comparing models of channel flow utilise the full Saint Venant equations including friction terms and variable river bed topography. The solution to these full equations is tested to convergence in extreme flow conditions and then compared with analytical solutions.

The L_1 norm was used for convergence (stopping) criteria, where subsequent iteration results are compared, and also for error comparisons with the analytical solutions. The L_∞ norm does not necessarily go to zero uniformly for discontinuous functions when the mesh size decreases. The L_2 norm has higher-order convergence and can be used for linearized equations, but the L_1 norm is the more natural and popular for modelling conservation laws [13].

5.1. Dam-break problems

The performance of the schemes was first tested on a idealised one-dimensional dam-break problem. The dam is initially located at the middle of a 2000-m long rectangular and frictionless channel. The water depth ratio is h_d/h_u where h_u is the upstream depth and h_d is the downstream depth. The governing equations are given by (1) with $\mathbf{G} = 0$. A grid of 400 points in space was used for the numerical simulation. The upstream depth h_u was kept constant at 10 m while the downstream depth h_d was different for each problem. When the depth ratio is greater than 0.5, the flow throughout the channel remains subcritical. The flow downstream is supercritical for depth ratios smaller than 0.5, while remaining subcritical upstream. The time increment is calculated to maintain a predetermined CFL number at the end of each time step and the flow conditions are computed to time 50 s. The analytical solutions for the sample problems are calculated using Stoker's [14] method and shown as a solid line in all figures.

All four schemes accurately predict the solution to the dam-break problem, for depth ratios of 0.05 and examples are given in Figures 1 and 2. This is partly due to each scheme running with a CFL number of one. Freezing the results at 50 s and therefore, without any convergence criteria, does not allow much distinction between the four TVD schemes or the Roe scheme. Inclusion of the Roe scheme allows comparison with a first-order scheme, a predecessor of the TVD schemes. Roe's scheme is normally the fastest with a low operation count and no limiter.

© 1998 John Wiley & Sons, Ltd.

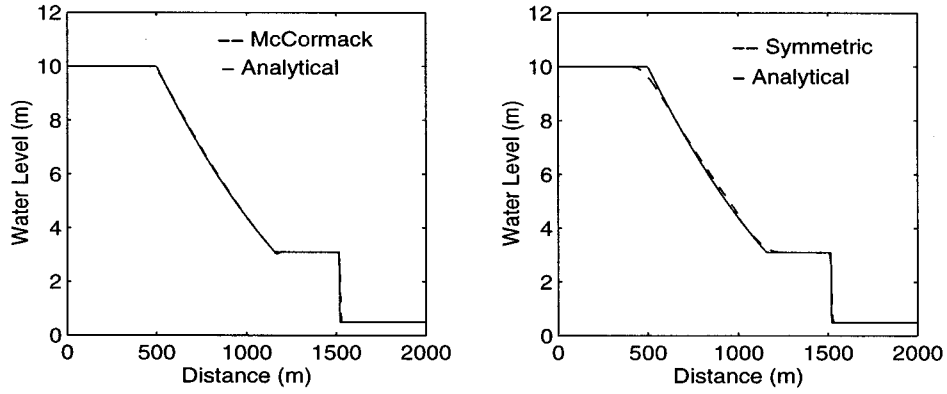

Figure 1. Dam-break results for symmetric and TVD–McCormack; depth ratio = 0.05.

The symmetric scheme gives the largest error in predicting the depression wave and the bore, as shown in Figure 3. For the most stringent case of depth ratio 0.0001, the symmetric scheme could not predict the solution for a CFL number of one; Figure 5 instead shows the symmetric scheme results for a CFL number of 0.95. The spurious oscillation exhibited at the wave front could cause total instability for the severe case with a CFL number of one. In comparison with upwind schemes, symmetric schemes do not give good results at contact discontinuities [6], such as the bore created with a dam-break.

The TVD–McCormack scheme was very accurate for depth ratio 0.005 (Figure 3), but for the most demanding case, depth ratio 0.0001, it gives an oscillatory overshoot in predicting the wave front, as illustrated in Figure 5. Unlike the symmetric scheme, the TVD–McCormack was not totally unstable with CFL number of one.

The modified flux predicts flow well for all depth ratios with a CFL number of one. Figure 6 illustrates that Yee's modified flux method yields useful results for a very small depth ratio, in contrast to Harten's method [15].

The third-order MUSCL scheme does not give the oscillations associated with the second-order MUSCL scheme for CFL number of one [15] and it gives similar results to the modified flux, although it is better at predicting the wave front. The greatest accuracy is predicted with the only third-order scheme presented. Results for these two schemes for depth ratios 0.005 and 0.0001 are shown in Figures 4 and 6.

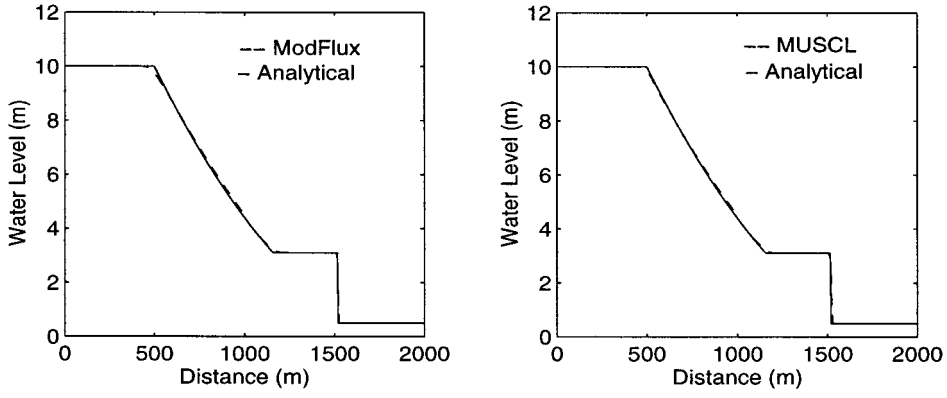

Figure 2. Dam-break results for modified flux and MUSCL; depth ratio = 0.05.

© 1998 John Wiley & Sons, Ltd.

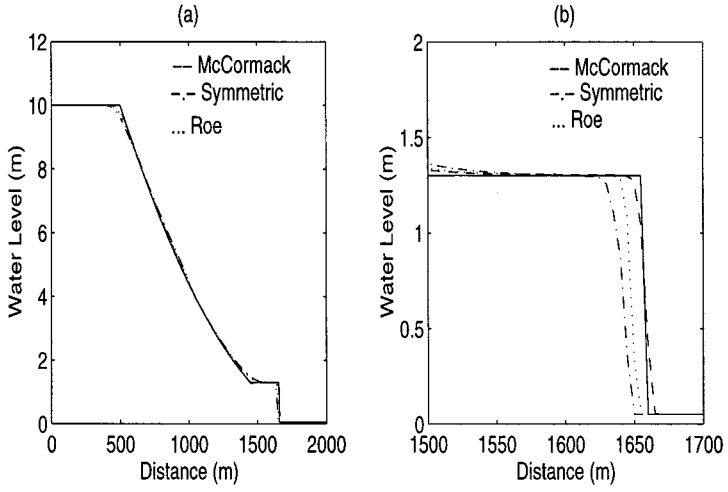

Figure 3. (a) Comparison of symmetric, Roe and TVD–McCormack, (b) enlargement of the wave front; depth ratio = 0.005.

In each case, the smooth water profile indicates that the automatically calculated entropy condition is operating as intended, with no unrealistic jumps predicted.

5.2. Variable river bed topography

In order to make more realistic comparisons between the schemes for modelling channel flow, the friction components must be incorporated. The governing equations again are given by (1), with **G** given by (4). MacDonald *et al.* [16] provide examples with analytical solutions. Their two most demanding problems contain hydraulic jumps. Our first example, problem 1, has a subcritical inflow and outflow with a supercritical central section. The second, problem 2, has a supercritical inflow and outflow with a subcritical central section. The analytical solutions representing the water level are plotted in Figure 7.

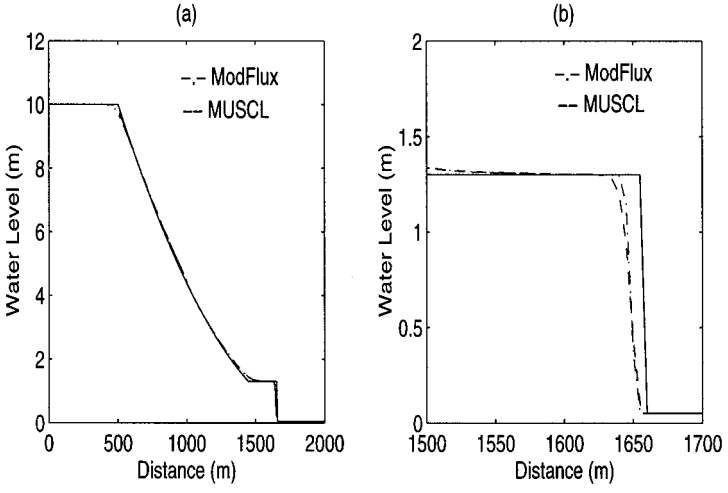

Figure 4. (a) Comparison of modified flux and MUSCL, (b) enlargement of the wave front; depth ratio = 0.005.

© 1998 John Wiley & Sons, Ltd.

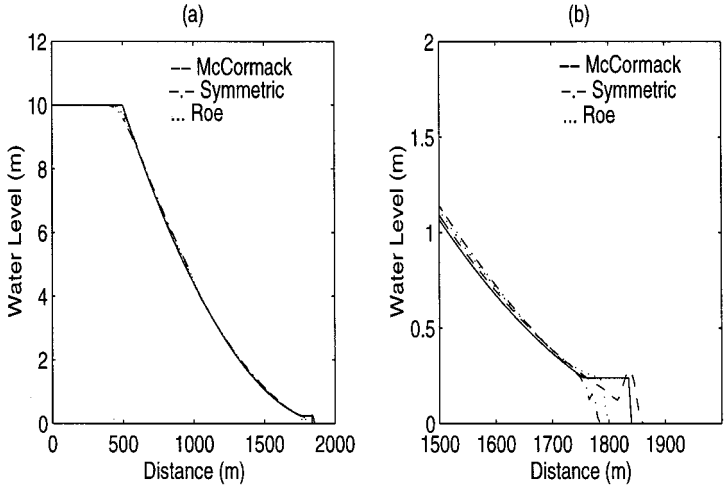

Figure 5. (a) Comparison of symmetric, Roe and TVD–McCormack, (b) enlargement of the wave front; depth ratio = 0.0001.

Both examples have rectangular channels 100 m long and 10 m wide. Both use an inflow discharge of 20 $m^3\ s^{-1}$ and Manning's roughness coefficient is constant at 0.03. A grid of 100 points in space has been used for the numerical simulations for each problem. The time increment is again computed, to maintain a constant CFL number at the end of each time step until convergence is achieved. The type of flow in the two examples is determined by their variable bed slopes, S_0, which are given as functions of the exact water depths and their derivatives (see Appendix). The analytical solutions are plotted with a solid line in all figures.

Before enlargement, each of the numerical predictions of channel flow again appear to be accurate, as shown in Figures 8 and 10 for problem 1 and Figures 12 and 14 for problem 2. A CFL number of one can be used for all the schemes except for (i) the modified flux, in modelling both sample problems and (ii) the MUSCL in modelling problem 1. In these cases,

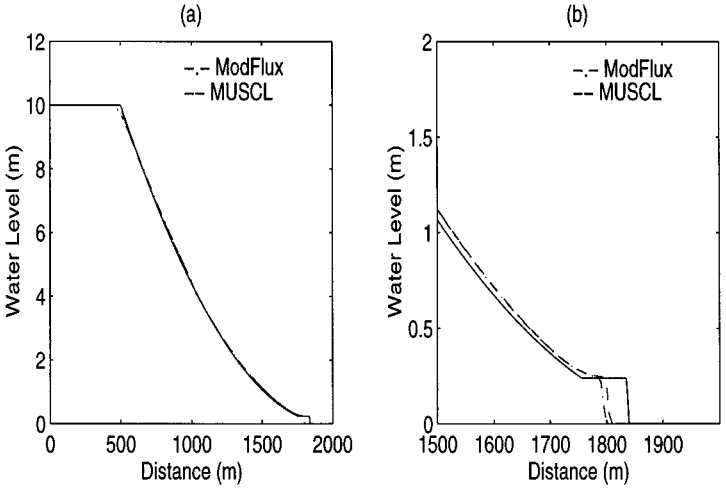

Figure 6. (a) Comparison of modified flux and MUSCL (b) enlargement of the wave front; depth ratio = 0.0001.

© 1998 John Wiley & Sons, Ltd.

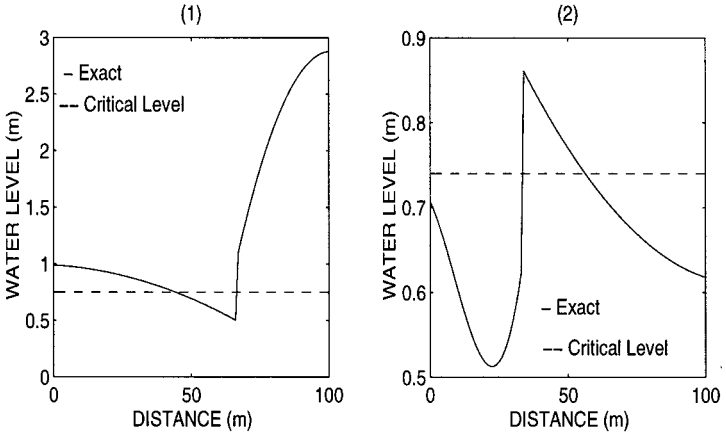

Figure 7. Analytical (exact) solutions for test problems 1 and 2.

the CFL number was set to 0.6. The solutions given by these two schemes produce similar water surface profiles, though in the second example the modified flux is less accurate in the smooth region than the third-order MUSCL. In fact, MUSCL has the lowest error of all the schemes in solving the Saint Venant equations for problem 2.

Compared with the other schemes, the Roe scheme badly clips the peak of the hydraulic jump in both problems, as shown in Figures 11 and 13. This is due to the accuracy lost with the smearing by the numerical diffusion associated with a first-order scheme. The symmetric scheme is very accurate in predicting the discontinuities, especially for the first problem, as shown in Figure 10. This scheme however loses accuracy in the smooth regions.

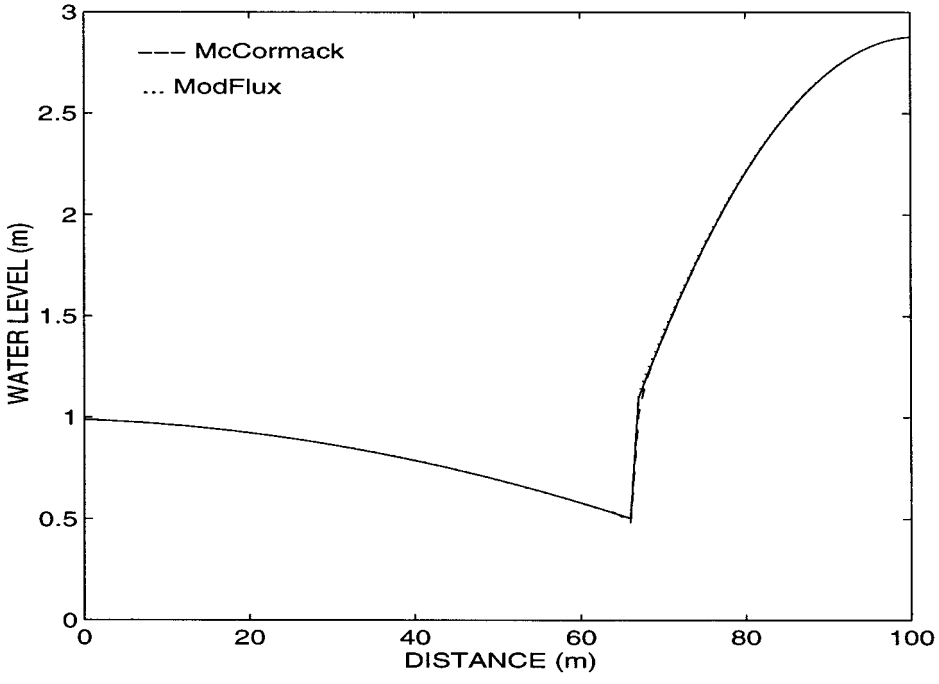

Figure 8. Numerical solution against exact solution for problem 1.

© 1998 John Wiley & Sons, Ltd.

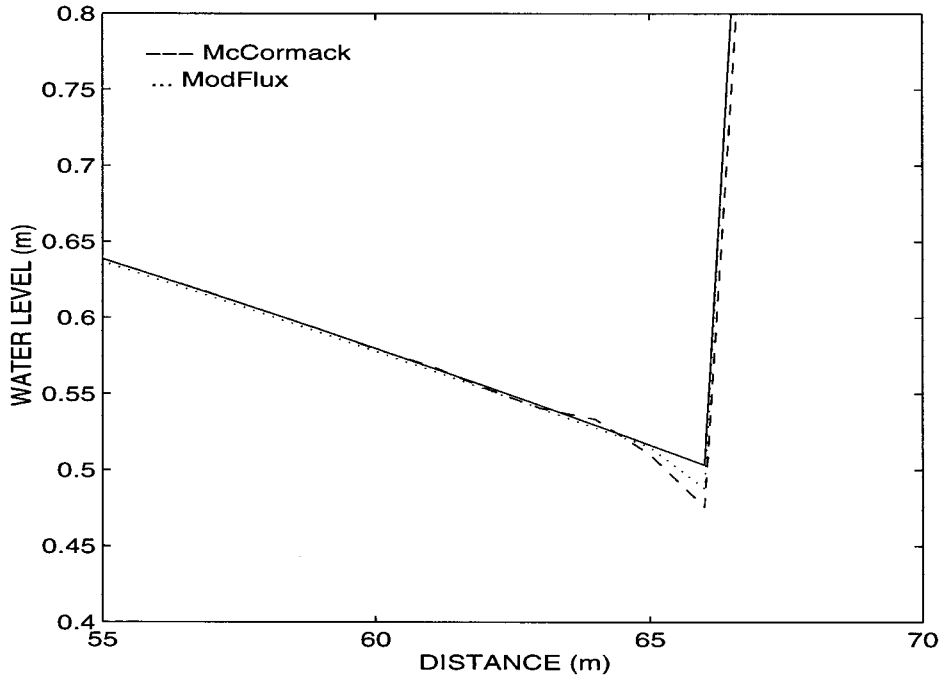

Figure 9. Magnified shock region from Figure 8.

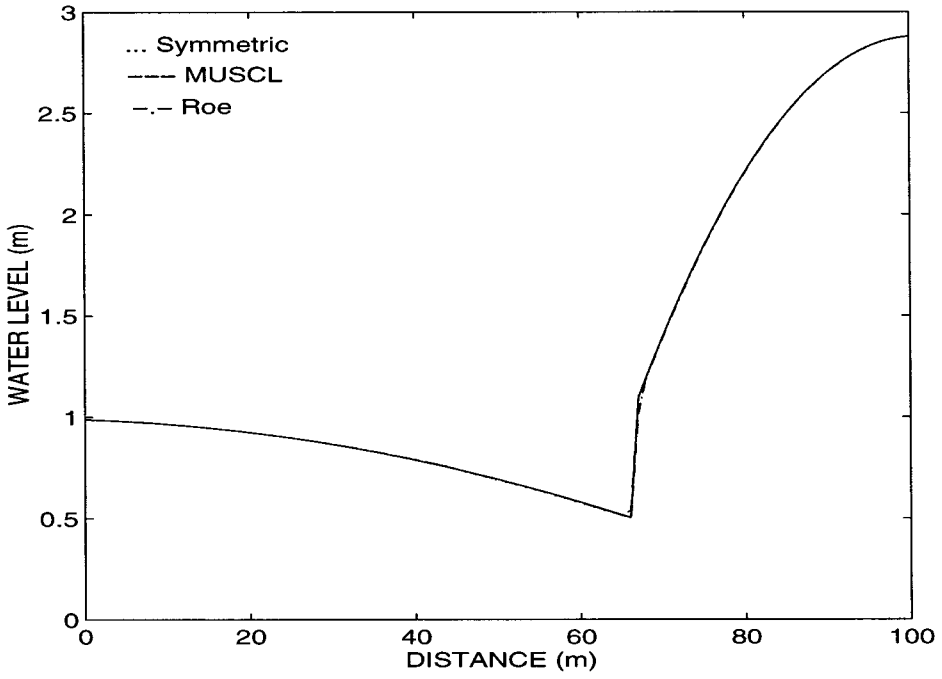

Figure 10. Numerical solutions against exact solution for problem 1.

© 1998 John Wiley & Sons, Ltd.

With a CFL number of one, the TVD–McCormack scheme oscillates about the shock and overshoots the shock prediction, as shown in Figures 9 and 15. Tests using other limiters, for example VanLeer's and Superbee [10,11] to dampen the oscillations, produced larger oscillations than produced with the minmod limiter.

We have found that the combination of arithmetic averages chosen to represent the source terms provides more accurate results than pointwise evaluation. Further work, however, is required to analyse the consistency and performance of other source term discretisations (e.g. Glaister [4]) for individual schemes.

6. CONCLUSIONS AND FURTHER WORK

All the schemes presented were accurate examples of their types and may be used to predict channel flow with hydraulic jumps. There are, however, variations between them.

Roe's scheme is the most popular and has the lowest computational cost, but its first-order properties manifest themselves in sizeable clipping of peaks at the hydraulic jumps (especially obvious in problem 2 of variable bed topography).

The most accurate prediction of the shock in problem 1 is with the symmetric scheme, but this is the least accurate scheme for non-transcritical flow. For problem 1, the modified flux and third-order MUSCL schemes require a comparatively low CFL number and produce similar results to each other. These schemes do not converge for high CFL numbers. This may be due to oscillations, which lower CFL numbers dampen.

The TVD–McCormack scheme gives accurate predictions with low error. However, the most severe dam-break case and the examples using the full equations show oscillations and a large overshoot in predicting the shock.

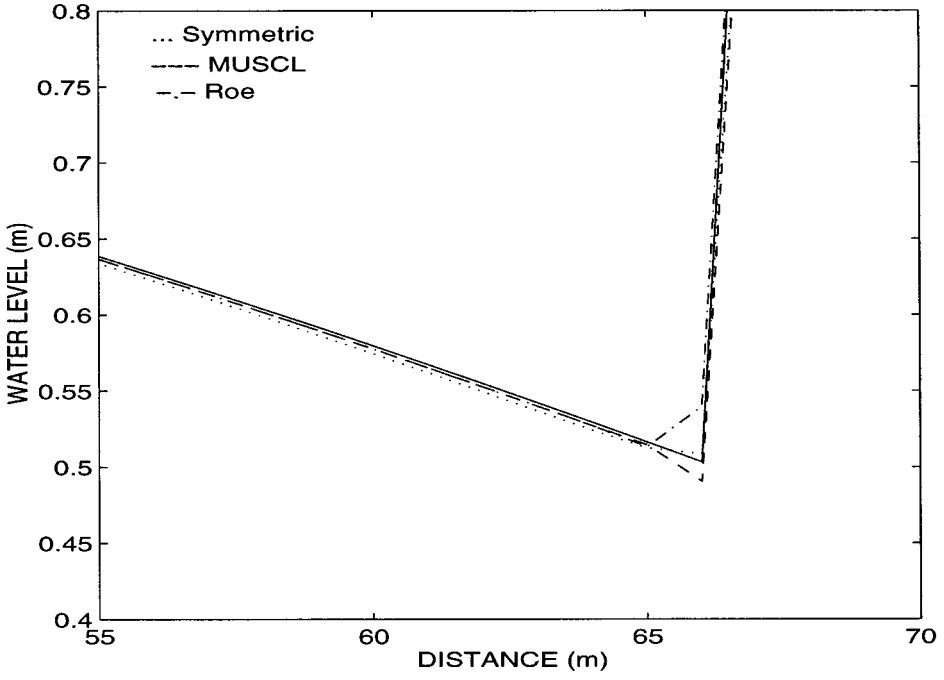

Figure 11. Magnified shock region from Figure 10.

© 1998 John Wiley & Sons, Ltd.

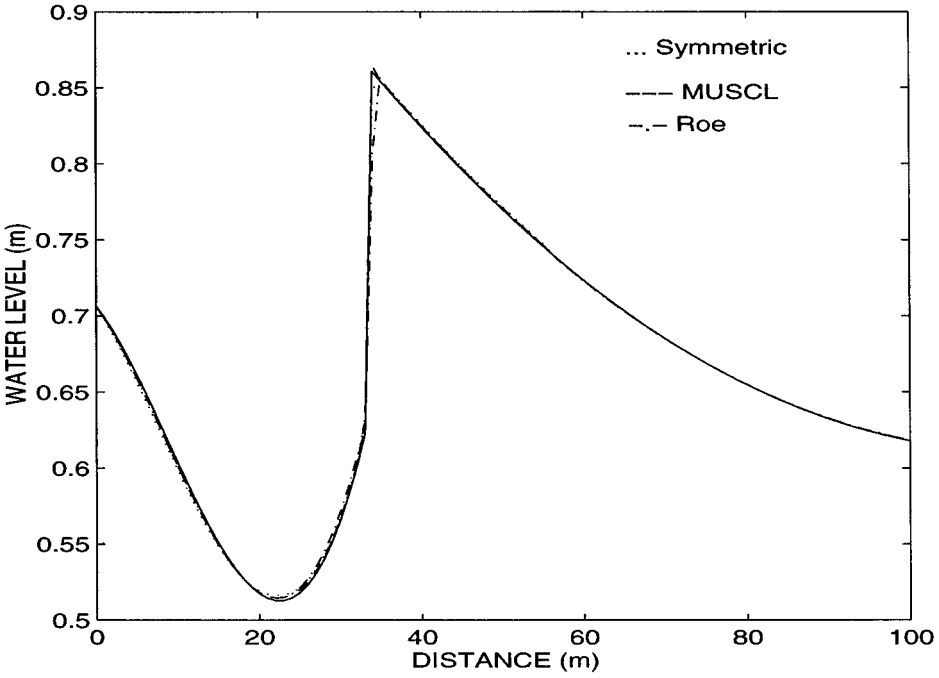

Figure 12. Numerical solutions against exact solution for problem 2.

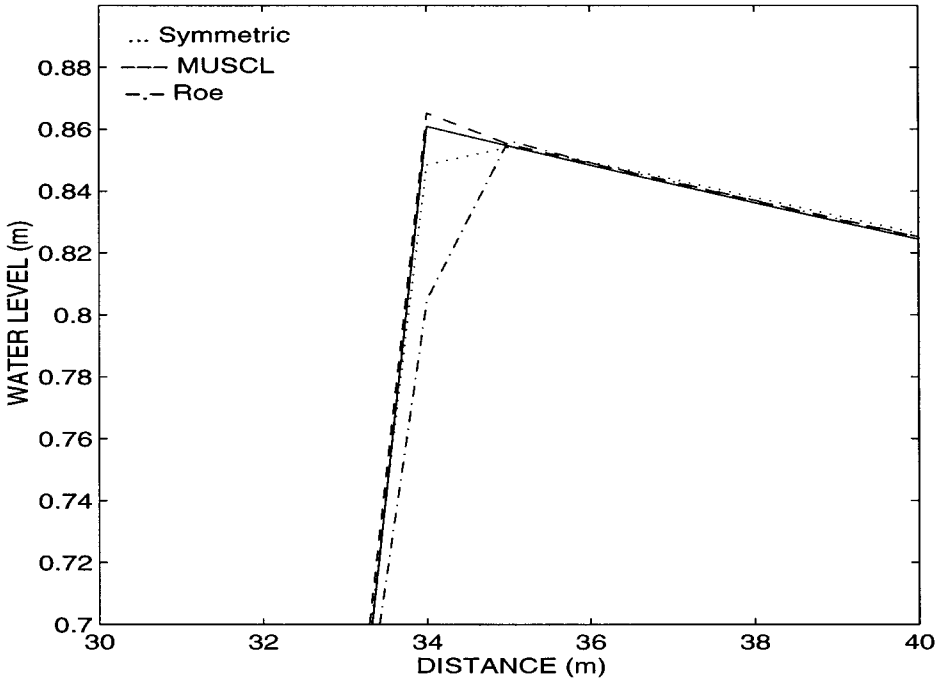

Figure 13. Magnified shock region from Figure 12.

© 1998 John Wiley & Sons, Ltd.

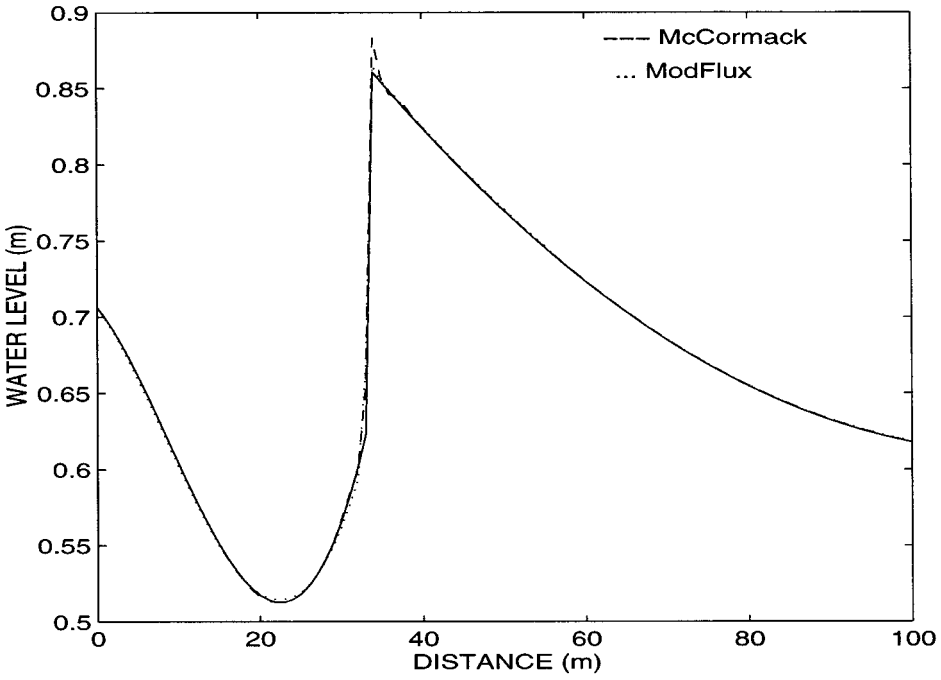

Figure 14. Numerical solutions against exact solution for problem 2.

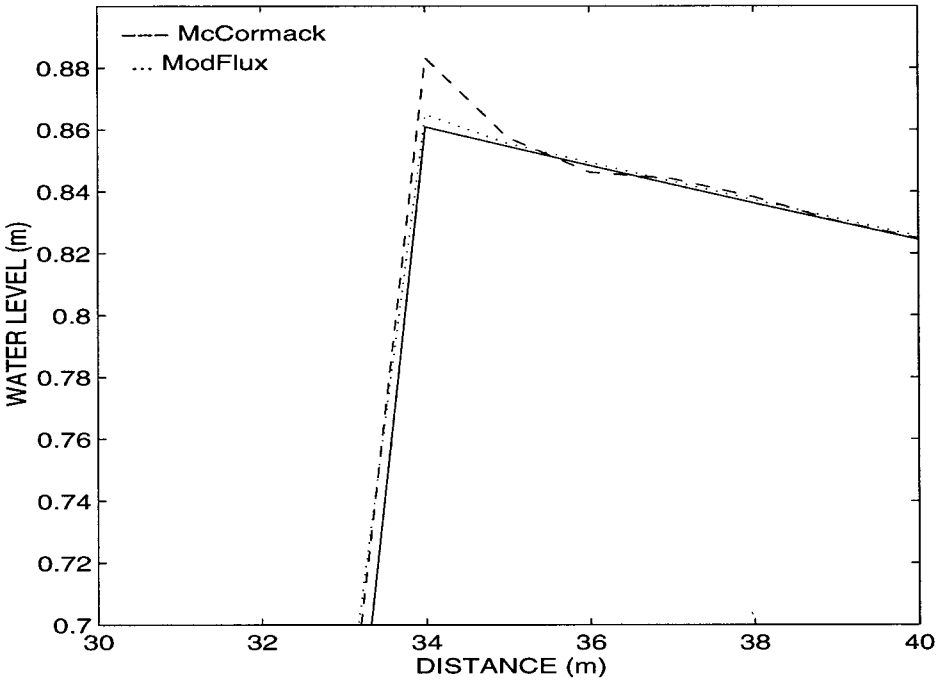

Figure 15. Magnified shock region from Figure 14.

© 1998 John Wiley & Sons, Ltd.

When an upwind scheme is the most appropriate, the third-order MUSCL scheme gives the most accurate results, with a slight improvement on second-order upwind schemes. However, the sub–super–subcritical problem presented is mostly accurately predicted with the symmetric scheme.

A variable time increment allows a high CFL number, supplying both fast and accurate results, and should therefore be used for every TVD scheme. The use of the automatically calculated entropy condition, which consistently chooses the correct physical solution producing smooth water profiles, is also recommended. Flow is more accurately simulated if the source terms are presented by arithmetic averages, rather than pointwise.

Further improvement in capturing the hydraulic jump requires more in depth experimentation with various limiters and a full analysis of the discretisation of the source terms. Though dam-break examples give an idea of comparative performance of the schemes, all schemes should be tested to convergence against analytical solutions containing friction and slope terms.

APPENDIX A

The slopes and analytical solutions for problems 1 and 2 in Section 5.2 are given here following MacDonald *et al.* [16].

A.1. Problem 1. Sub–super–subcritical flow with hydraulic jump

The slope of the channel is given by

$$S_0(x) = \left(1 - \frac{4}{g[h(x)]^3}\right)h'(x) + \frac{9}{2500[h(x)]^2}\left(\frac{1}{5} + \frac{1}{h(x)}\right)^{4/3},$$

where

$$h(x) = \begin{cases} \left(\dfrac{4}{g}\right)^{1/3}\left(\dfrac{4}{3} - \dfrac{x}{100}\right) - \dfrac{9x}{1000}\left(\dfrac{x}{100} - \dfrac{2}{3}\right) & x \le \dfrac{200}{3} \\ \left(\dfrac{4}{g}\right)^{1/3}\left(0.674202\left(\dfrac{x}{100} - \dfrac{2}{3}\right)^4 + 0.674202\left(\dfrac{x}{100} - \dfrac{2}{3}\right)^3\right. & \\ \left. - 21.7112\left(\dfrac{x}{100} - \dfrac{2}{3}\right)^2 + 14.492\left(\dfrac{x}{100} - \dfrac{2}{3}\right) + 1.4305\right) & x > \dfrac{200}{3} \end{cases}$$

and

$$h'(x) = \begin{cases} \dfrac{-1}{100}\left(\dfrac{4}{g}\right)^{1/3} - \dfrac{9}{500}\left(\dfrac{x}{100} - \dfrac{1}{3}\right) & x \le \dfrac{200}{3} \\ \left(\dfrac{4}{g}\right)^{1/3}\left(0.02696808\left(\dfrac{x}{100} - \dfrac{2}{3}\right)^3 + 0.02022606\left(\dfrac{x}{100} - \dfrac{2}{3}\right)^2\right. & \\ \left. - 0.434224\left(\dfrac{x}{100} - \dfrac{2}{3}\right) + 0.14492\right) & x > \dfrac{200}{3}. \end{cases}$$

© 1998 John Wiley & Sons, Ltd.

The flow is subcritical at inflow and outflow. Hence, the boundary conditions are inflow discharge of 20 $m^3\ s^{-1}$ and $h(100)$. The exact depth for this problem is given by $h(x)$.

A.2. Problem 2. Super–sub–supercritical flow with hydraulic jump

The slope of the channel is given by

$$S_0(x) = \left(1 - \frac{4}{g[h(x)]^3}\right)h'(x) + \frac{9}{2500[h(x)]^2}\left(\frac{1}{5} + \frac{1}{h(x)}\right)^{4/3},$$

where

$$h(x) = \begin{cases} \left(\frac{4}{g}\right)^{1/3}\left(-10.7872\left(\frac{x}{100} - \frac{1}{3}\right)^4 + 18.8777\left(\frac{x}{100} - \frac{1}{3}\right) + 17.9329\left(\frac{x}{100} - \frac{1}{3}\right)^2 \right. & x \le \frac{200}{3} \\ \left. + 3.1725\left(\frac{x}{100} - \frac{1}{3}\right) + 0.850042\right) & \\ \left(\frac{4}{g}\right)^{1/3}\left(\frac{5}{6} + \frac{(100-x)}{200}\right) + \frac{4}{10}\left(\frac{x}{100} - \frac{1}{3}\right)\left(\frac{x}{100} - 1\right) & x > \frac{200}{3} \end{cases}$$

and

$$h'(x) = \begin{cases} \left(\frac{4}{g}\right)^{1/3}\left(-4.31488\left(\frac{x}{100} - \frac{1}{3}\right)^3 + 0.566331\left(\frac{x}{100} - \frac{1}{3}\right)^2 \right. & x \le \frac{200}{3} \\ \left. + 0.358658\left(\frac{x}{100} - \frac{1}{3}\right) + 0.031725\right) & \\ \frac{-1}{200}\left(\frac{4}{g}\right)^{1/3} + \frac{4}{500}\left(\frac{x}{100} - \frac{2}{3}\right) & x > \frac{200}{3} \end{cases}$$

The flow is supercritical at inflow and outflow. Hence, the boundary conditions are inflow discharge of 20 $m^3\ s^{-1}$ and $h(0)$. The exact depth for this problem is given by $h(x)$.

REFERENCES

1. J.A. Cunge, F.M. Holly and A. Verway, *Practical Aspects of Computational River Hydraulics*, Pitman, London, 1980.
2. P.L. Roe, 'Approximate Riemann solvers, parameter vectors, difference schemes', *J. Comput. Phys.*, **43**, 357–372 (1981).
3. S.K Godunov, 'A difference method for the numerical computation of continuous solutions of hydrodynamic equations', *Mat. Sbornik*, **47**, 271–306 (1959) (Translated as JPRS by US DEPT of Commerce, 1960).
4. P. Glaister, 'Flux difference splitting for open-channel flows', *Int. j. numer. methods fluids*, **16**, 629–654 (1993).
5. A. Harten, 'High-resolution schemes for hyperbolic conservation laws', *J. Comput. Phys.*, **49**, 357–393 (1983).
6. H.C. Yee, 'A class of high-resolution explicit and implicit shock-capturing methods', *NASA-TM 101088*, 1989.
7. A. Harten and J.M. Hyman, 'Self adjusting grid method for one-dimensional hyperbolic conservation laws', *J. Comput. Phys.*, ***50***, 235–296 (1983).
8. A. Harten, 'On a class of high-resolution total variation stable finite difference schemes', *SIAM J. Numer. Anal.*, **21**, 1–23 (1984).
9. C. Hirch, 'Numerical computation of internal and external flows', in Vol. 2, *Computational Methods for Inviscid and Viscous Flows*, Wiley, Chichester, 1990.
10. P. Garcia-Navarro and F. Alcrudo, 'Implicit and explicit TVD methods for discontinuous open channel flows', in R.A. Falconer, K. Shiono and R.G.S. Matthew (eds.), *Proc. of the 2nd Int. Conf. on Hydraulic and Environmental Modelling of Coastal, Estuarine and River Waters, Vol.* 2, 1992.

© 1998 John Wiley & Sons, Ltd.

11. P.K. Sweby, 'High resolution schemes using flux limiters for hyperbolic conservation laws', *SIAM J. Numer. Anal.*, **21**, 995–1011 (1984).
12. B. Van Leer, 'Towards the ultimate conservation difference scheme V, a second order sequel to Godunov's method', *J. Comput. Phys.*, **32**, 101–136 (1979).
13. R.J. LeVeque, 'ETH Zurich lectures in mathematics', in *Numerical Methods for Conservation Laws*, Birkhauser, Basel, 1990
14. J.J. Stoker, *Water Waves*, Interscience, New York, 1957.
15. A.K. Jha, J. Akiyama and M. Ura, 'First and second order flux difference splitting schemes for dam-break problem', *J. Hydraulic Eng.*, **121**, 877–884 (1995).
16. I. MacDonald, M.J. Baines and N.K. Nichols, 'Analysis and computation of steady open channel flow using a singular perturbation problem', *Numererical Analysis Report* 7/94, University of Reading, 1994.

© 1998 John Wiley & Sons, Ltd.